Tropical Cyclone Motion in a Nondivergent Barotropic Model

MARK DEMARIA*

*National Center for Atmospheric Research,** Boulder, CO 80307*

(Manuscript received 29 October 1984, in final form 15 March 1985)

ABSTRACT

Tropical cyclone motion is investigated in the context of a nondivergent barotropic model. For this purpose, the nondivergent barotropic vorticity equation is solved on a doubly-periodic midlatitude β-plane using a spectral method with Fourier basis functions. The results from previous studies are summarized and illustrated in idealized model simulations. It is shown that the absolute vorticity gradient of the steering current ($\nabla\bar{\zeta}_a$) causes an axisymmetric vortex to drift relative to the steering current with a component in the direction of the gradient and a component 90° to the left of the gradient. The implications of the basic principles of vortex motion for operational track prediction models are discussed. By consideration of the horizontal variation of $\nabla\bar{\zeta}_a$, it is shown that a vortex track will be more sensitive to initial position errors in regions where $\nabla^2\bar{\zeta}_a > 0$ than in regions where $\nabla^2\bar{\zeta}_a < 0$. It is also shown that the vortex track is much more sensitive to changes in the outer regions (size changes) than to changes in the inner regions (intensity changes) of the vortex, and that the vortex track is more sensitive to size changes in regions where $|\nabla\bar{\zeta}_a|$ is large.

The effect of numerical approximation on the vortex track is studied by comparing the spectral model to a second-order finite difference version of the model. These results suggest that the resolution used in some operational tropical cyclone track prediction models is inadequate.

1. Introduction

The first attempts at predicting tropical cyclone tracks using dynamical methods were made in the 1950s (e.g., Sasaki, 1955; Kasahara, 1957). Because of the limited computational resources it was necessary to use simple barotropic models and to treat the small-scale vortex circulation separately from the larger-scale flow. As a consequence of this approach, much insight was gained about the basic processes which affect the motion of vortices in these simplified models. As computing power increased it was no longer necessary to treat the vortex separately (e.g., Birchfield, 1960; Sanders and Burpee, 1968) and eventually, multilevel primitive equation models were used for operational track prediction (Hovermale and Livezey, 1977; Harrison, 1981).

Although there are some situations where tropical cyclone motion can only be modeled using primitive equations (for example, when a vortex interacts with a vertically-sheared basic current), there is evidence that some aspects of tropical cyclone motion can be described with simpler barotropic models. For example, the current operational version of the SANBAR model is governed by a barotropic vorticity equation and is initialized with the nondivergent part of the horizontal wind vertically-averaged from 1000 to 100 mb. In a comprehensive comparison of dynamical and statistical forecast methods, Neumann and Pelissier (1981b) have shown that the SANBAR model is superior to other forecast methods for medium range track forecasts of low-latitude Atlantic tropical cyclones. In the Australian/Southwest Pacific region, Holland (1983, 1984) has shown that many aspects of tropical cyclone motion can be explained using a theory based on a barotropic vorticity equation. Chan (1984) has calculated the terms in the full form of the vorticity equation using aircraft and rawinsonde composite data. These results show that the dominant contribution to the local vorticity change in the region near the tropical cyclone center comes from the horizontal advection term.

These earlier results indicate the importance of vorticity conservation for the motion of tropical cyclones. The simplest model which contains this effect is governed by the nondivergent barotropic vorticity equation. In this paper, the motion of tropical cyclones is investigated in this context. For this purpose, the nondivergent barotropic vorticity equation is solved on a doubly-periodic midlatitude β-plane using a spectral method with Fourier basis functions. A brief description of the model is given in Section 2. In Section 3, the basic principles of tropical cyclone motion found in previous studies are summarized and illustrated in idealized model simulations. In Section 4, the implications of these basic principles for operational track prediction are discussed. In Section 5, the effect of numerical approx-

* Current affiliation: Dept. of Marine, Earth and Atmospheric Sciences, North Carolina State University, Raleigh, NC 27695.

** The National Center for Atmospheric Research is sponsored by the National Science Foundation.

imation on the motion of a tropical cyclone is investigated. For this purpose, a second-order finite difference version of the model is run with the resolution used in operational models and the results are compared to a high resolution spectral version of the model.

2. Model description

The governing equation for this model is the conservation of absolute vorticity on a midlatitude β-plane which can be written as

$$\frac{\partial \zeta}{\partial t} + \frac{\partial}{\partial x}(u\zeta) + \frac{\partial}{\partial y}(v\zeta) + \beta v = 0, \qquad (2.1)$$

where ζ is the vertical component of the relative vorticity, u and v the eastward and northward components of the nondivergent wind, and β the northward gradient of the Coriolis parameter. In (2.1), ζ can be related to the horizontal wind components by introducing a streamfunction ψ where

$$\zeta = \frac{\partial^2 \psi}{\partial x^2} + \frac{\partial^2 \psi}{\partial y^2}, \qquad (2.2)$$

$$u = -\frac{\partial \psi}{\partial y}, \quad v = \frac{\partial \psi}{\partial x}. \qquad (2.3)$$

In most of the simulations which will be presented, (2.1)–(2.3) were solved using a spectral method with Fourier basis functions on a doubly-periodic domain. For this purpose, the dependent variables are expanded in double-Fourier series, and substituted into (2.1)–(2.3). The standard Galerkin procedure is then applied which gives equations for the time-dependent series amplitudes. The spectral form of (2.1) is solved using the second-order Adams-Bashforth time differencing scheme. A more detailed description of this numerical method can be found in DeMaria and Schubert (1984) in the context of a three-dimensional model. Unless otherwise indicated, the model was truncated at wavenumber 47 in the x and y directions on 4000 km square domain. The smallest wave in the model then has a wavelength of about 85 km.

In Section 5, some results from a finite difference version of the model will be presented. For this case, a doubly-periodic 4000 km square domain is again used. The nonlinear advective terms in (2.1) are evaluated using the second-order difference method described by Arakawa (1966), which conserves mean kinetic energy and mean square vorticity for the case with $\beta = 0$. The βv term is calculated using a centered difference and the elliptic equation (2.2) is solved using centered differences and then inverting the resulting linear system using a standard over-relaxation procedure. Similar to the spectral version of the model, second-order Adams-Bashforth time differencing is used.

3. Motion of an axisymmetric vortex

The motion of an axisymmetric vortex in the nondivergent barotropic model has been investigated by numerous authors in the 1950s and 1960s, using various assumptions and approximations. In this section, the results of these previous studies are compared with results from idealized numerical simulations.

The vortex considered here is defined by

$$V = 2V_m(r/r_m)\frac{\exp[-a(r/r_m)^b]}{1 + (r/r_m)^2}, \qquad (3.1)$$

where V is the tangential wind, r the radial distance from the vortex center, V_m the approximate maximum tangential wind (exact for $a = 0$), and r_m the approximate radius of maximum wind. The exponential factor in (3.1) is added so that V decays rapidly with r at large radii. Figure 1 shows V as a function of r with $V_m = 30$ m s^{-1}, $r_m = 80$ km, $a = 10^{-6}$, and $b = 6$. The dashed lines in Fig. 1 show the azimuthally-averaged tangential winds at 850 mb for large (L) and small (S) Atlantic hurricanes, obtained from Merrill (1984). The parameters in (3.1) were chosen so that the tangential wind profile outside the radius of maximum wind would come between the observed profiles for the large and small hurricanes.

a. Linear steering current

Most early attempts to determine tropical cyclone tracks were based on simple steering current principles (e.g., Riehl and Burgner, 1950). For this purpose, it is assumed that a small-scale tropical cyclone follows the motion of the surrounding large-scale flow field. This effect can be seen by considering (2.1) with $\beta = 0$. Now, suppose the axisymmetric vortex defined by (3.1) is imbedded in a constant flow with horizontal wind components $\bar{u}$ and $\bar{v}$. It can be shown that for an axisymmetric vortex, the two nonlinear advective terms cancel, so that with $\beta = 0$, (2.1) becomes

$$\frac{\partial \zeta}{\partial t} + \bar{u}\frac{\partial \zeta}{\partial x} + \bar{v}\frac{\partial \zeta}{\partial y} = 0, \qquad (3.2)$$

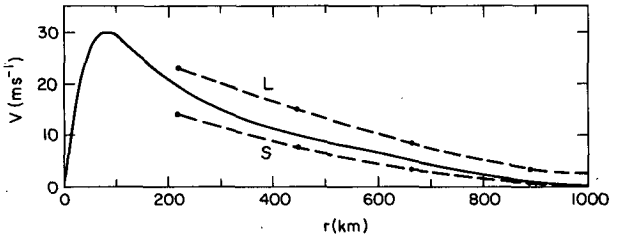

FIG. 1. The tangential wind V as a function of radius r for the vortex defined by (3.1) with $V_m = 30$ m s^{-1}, $r_m = 80$ km, $a = 10^{-6}$ and $b = 6$ (solid curve). The dashed lines show the azimuthally-averaged 850 mb tangential winds for large (L) and small (S) Atlantic hurricanes.

where ζ represents the vorticity of the vortex, since the vorticity of the constant flow is zero. Equation (3.2) is a two-dimensional constant coefficient linear advection equation which indicates that the vorticity field of the vortex moves with the basic flow. This result has been derived in many previous studies (e.g., Kasahara, 1957; Adem and Lezama, 1960).

If an axisymmetric vortex is added to a sheared current, the vorticity field of the vortex will soon become asymmetric due to differential vorticity advection by the current. Once the vortex becomes asymmetric, the nonlinear advection terms in (2.1) will no longer cancel, so that the motion of the vortex will no longer be governed by a linear advection equation of the form of (3.2). If the shear of the current is linear, there will be no vorticity gradients associated with it, so that the steering current should not be advected by the vortex circulation. Thus, the shear of the steering current should remain linear. It might then be expected that although the vortex would become asymmetric, it would still move with the steering current at the vortex center.

The above hypothesis was verified using the spectral model. The axisymmetric vortex defined by (3.1) was added to a zonal current which varied linearly with y over most of the model domain. Although the vorticity field of the vortex became asymmetric, the vortex still moved with the speed of the zonal current at the vortex center. Thus, an axisymmetric vortex in the nondivergent barotropic model moves exactly with a constant or linearly-sheared basic current.

b. Steering current with a vorticity gradient

In the previous example, the axisymmetric vortex did not interact with the vorticity field of the steering current since there were no vorticity gradients associated with the current. When the basic current is a nonlinear function of x or y, or the gradient of the earth's vorticity is included ($\beta \neq 0$), the vortex can interact with the background vorticity field.

A simple example of the effect of background vorticity gradients is the effect of the gradient of the earth's vorticity on the motion of an axisymmetric vortex. Rossby (1948) argued that an axisymmetric cyclonic vortex should experience a net poleward acceleration because of the meridional gradient of the Coriolis force (the β-effect). As discussed by Anthes (1982, p. 108), Rossby's result did not include the effect of compensating pressure forces, so that it probably has little bearing on the long-term drift of a vortex. Adem (1956) studied the β-effect using a Taylor series solution to the nondivergent barotropic vorticity equation. These results show that a symmetric cyclonic vortex should move westward initially and then turn northward as higher-order time derivatives become important. This result has been confirmed in numerous modeling studies such as those by Anthes and Hoke (1975), Madala and Piacsek (1975), Jones (1977), and Kitade (1980, 1981), which showed that the β-effect causes model tropical cyclones to move towards the northwest at speeds between 1 and 3 m s^{-1}.

Figure 2 shows the track of the vortex defined by (3.1) during a 72-hour simulation of the spectral model with β evaluated at 20°N. The lower portion of this figure shows that the vortex accelerates towards the northwest during the first 24 hours. After this time, the vortex moves towards the northwest at a fairly constant speed of about 2.5 m s^{-1}.

Kuo (1950) generalized Rossby's argument to include the effects of relative vorticity gradients. The equation for the motion of an axisymmetric rotating cylinder in a current where the vorticity field has a discontinuity derived by Kuo (1969) shows that a cyclonic vortex should experience an acceleration in the direction of the relative vorticity gradient. In apparent contradiction to the results of Kuo, Sasaki (1955) and Kasahara (1957) showed that the relative vorticity gradient causes a vortex (either cyclonic or anticyclonic) to move in a direction 90° to the left of the direction of the vorticity gradient. In those studies, however, the effect of the vortex on the steering flow was neglected. In the study by Kasahara and Platzman (1963) this effect was included. These results showed that a cyclonic vortex will have a component of motion 90° to the left of the vorticity gradient as well as a component in the direction of the gradient. In their study the effects of the relative vorticity gradient and the earth's vorticity gradient

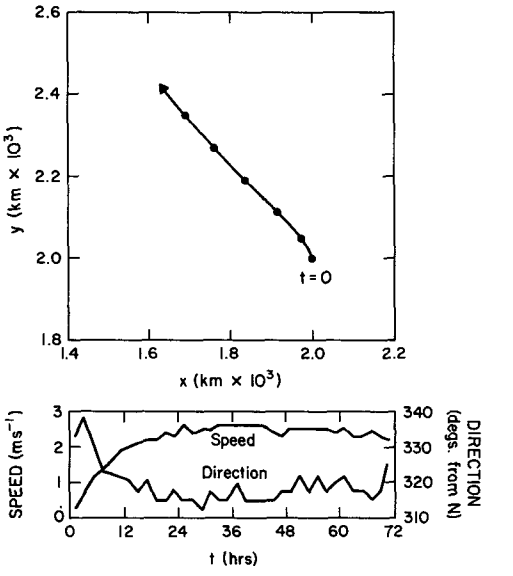

FIG. 2. The track of the axisymmetric vortex during a 72-hour simulation on the midlatitude β-plane, where the black dots indicate the positions at 12-hour intervals (upper panel). Also shown are the time evolution of the vortex speed and direction measured clockwise from north (lower panel).

were evaluated simultaneously by considering the absolute vorticity gradient.

To illustrate the effects of the relative vorticity gradient, consider a zonal current defined by

$$\bar{u}(y) = -10 \sin \frac{2\pi y}{L}. \qquad (3.3)$$

Figure 3 shows $\bar{u}(y)$ and the associated relative vorticity (normalized by the Coriolis parameter f at 20°N) and northward component of the relative vorticity gradient (normalized by β at 20°N) as a function of y for L = 4000 km. Now, consider an axisymmetric vortex initially centered at y_0 = 2750 km or y_0 = 1250 km (points A and B, respectively, shown in Fig. 3). At point A it can be seen that the relative vorticity gradient of the steering current is towards the north while at point B, it is towards the south. Neglecting the β-effect, the relative vorticity gradient should cause the vortex to drift towards the northwest at point A and towards the southeast at point B, relative to the steering current. The solid lines in Fig. 4 show the track of the axisymmetric vortex defined by (3.1) when placed at points A or B, where the model was run with $\beta = 0$. As expected from the previous discussion, the vortex initially at point A acquires a northward component to its motion, while the vortex at point B acquires a southward component to its motion. At t = 48 hours, the velocity components of the vortex initially at point A are u = 6.6 m s^{-1} and v = 1.8 m s^{-1}. At t = 48 hours, this vortex is at a position where the zonal current speed is 10 m s^{-1}. Thus, relative to the zonal current, the vortex has acquired a westward and northward component to its motion. Similarly, the vortex initially at point B acquires an eastward and southward component to its motion relative to the zonal current at the vortex center.

The dashed lines in Fig. 4 show the track of the axisymmetric vortex when placed at points A or B, where the model was run with β evaluated at 20°N. For this case, the absolute vorticity gradient must be considered. At point A, the relative vorticity gradient

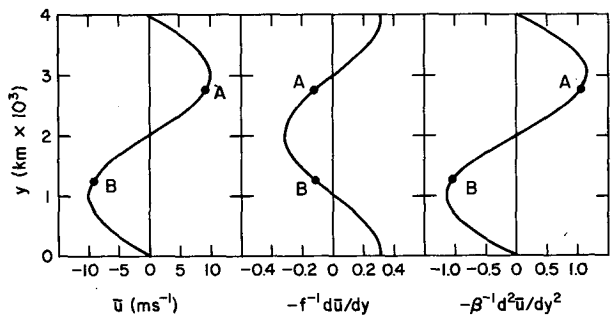

FIG. 3. The zonal wind profile defined by (3.3) (left panel) and the corresponding normalized relative vorticity (middle panel) and normalized relative vorticity gradient (right panel).

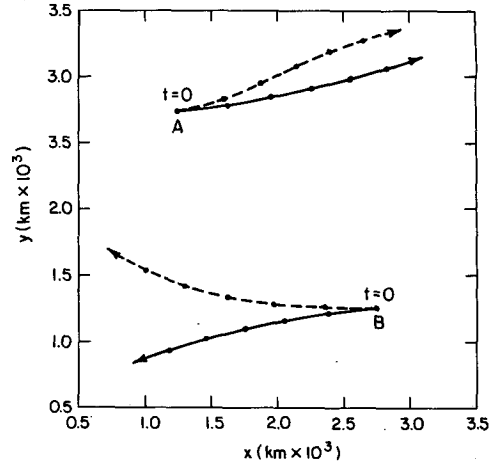

FIG. 4. The track of the axisymmetric vortex placed in the zonal wind profile defined by (3.3) on the f-plane (solid) and on the β-plane (dashed). The black dots indicate the positions at 12-hour intervals.

is in the same direction as the earth's vorticity gradient, so that the northwestward drift is enhanced, compared to the β = 0 case. At point B, however, the relative and earth's vorticity gradients are of opposite signs, so that the vortex moves almost due westward initially.

In summary, the above model simulations verify the results of Kasahara and Platzman (1963). The absolute vorticity gradient of the steering current results in a component of motion 90° to the left of the gradient, and a component in the direction of the gradient.

4. Implications for dynamical track prediction

In this section, the implications of the results of Section 3 for operational track prediction models are discussed.

a. Sensitivity to initial position errors

In the previous section it was shown that the drift of an axisymmetric vortex relative to the steering current depends on the absolute vorticity gradient of the steering current ($\nabla\bar{\zeta}_a$). Now, suppose a vortex is in a current where $\nabla\bar{\zeta}_a$ contains only a northward component and that $\nabla\bar{\zeta}_a$ increases towards the north. If a vortex was displaced towards the north, the northwestward drift of the vortex will be increased due to the increased $\nabla\bar{\zeta}_a$. The track of the displaced vortex would then have a larger northerly component to its motion than a vortex which was not displaced. It might then be expected that the track of the displaced vortex would diverge from the track of the vortex which was not displaced. By a similar argument, if $\nabla\bar{\zeta}_a$ decreased toward the north, the track of

the displaced vortex would converge with the track of the vortex which was not displaced.

To verify the above argument, consider a zonal current defined by

$$\bar{u}(y) = \bar{u}_m\left(\frac{y - y_0}{y_m}\right) \exp\left\{\frac{1}{2}\left[1 - \left(\frac{y - y_0}{y_m}\right)^2\right]\right\}, \quad (4.1)$$

where y_0 is the latitude where $\bar{u}$ changes sign and y_m is the distance from y_0 to the latitude of maximum zonal wind speed $\bar{u}_m$. Figure 5 shows $\bar{u}(y)$ and the associated normalized relative vorticity and northward component of the normalized relative vorticity gradient for the zonal wind profile given by (4.1) with y_0 = 2000 km, y_m = 600 km, and $\bar{u}_m$ = 10.0 m s^{-1} (solid) or $\bar{u}_m$ = −10.0 m s^{-1} (dashed). Now, suppose an axisymmetric vortex was positioned at points A, B, or C with $\bar{u}_m$ = −10.0 as shown in Fig. 5. From the first two panels, it can be seen that the vortex would be in a mean easterly current with anticyclonic wind shear in all three cases. The third panel shows that at positions A, B, or C, the relative vorticity gradient of the steering current is towards the north, zero, or towards the south, respectively. Similarly, at positions D, E, and F with $\bar{u}_m$ = 10.0 m s^{-1}, the vortex would be in a mean easterly current with cyclonic shear in all three cases, but the relative vorticity gradient of the current at positions D, E, or F is towards the north, zero, or towards the south, respectively. Thus, at each point, $\nabla\bar{\zeta}_a$ contains only a northward component ($\partial\bar{\zeta}_a/\partial y$), which increases towards the north at positions A–C and decreases towards the north at positions D–F.

Figure 6 shows the track of the axisymmetric vortex defined by (3.1) when placed in the zonal current at positions A–F, where β was evaluated at 20°N. This figure shows that the vortex tracks for initial positions A–C diverge, while the tracks for initial positions D–F converge. For example, at t = 0, position A is 400 km north of position C and position F is 400 km north of position D. After 72 hours, the difference between the positions of the point A and point C vortices has increased to 1330 km while the difference between the positions of the point D and point F vortices has decreased to 240 km.

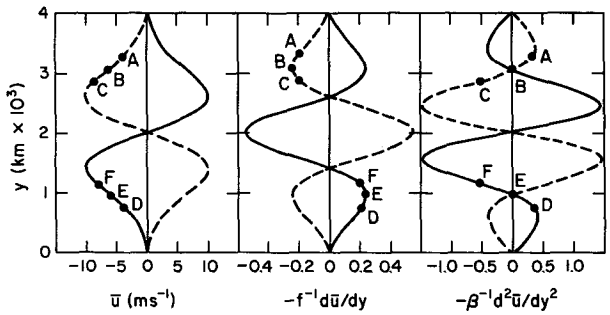

FIG. 5. As in Fig. 3 but for the zonal wind profile defined by (4.1) with y_0 = 2000 km, y_m = 600 km, and $\bar{u}_m$ = 10 m s^{-1} (solid) or $\bar{u}_m$ = −10 m s^{-1} (dashed).

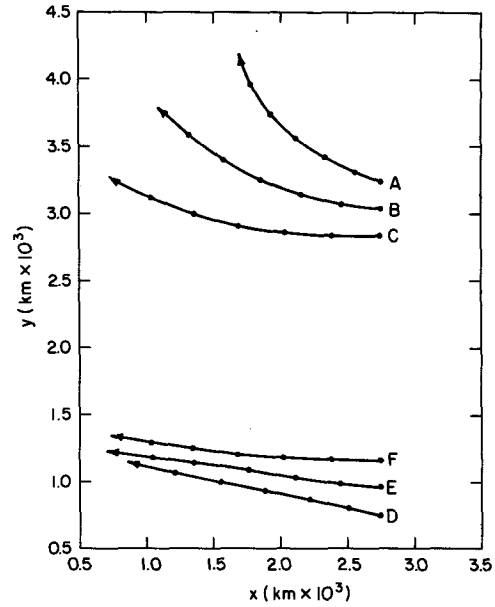

FIG. 6. The track of the axisymmetric vortex placed in the zonal current defined by (4.1) with $\bar{u}_m$ = −10 m s^{-1} (A, B, and C) or with $\bar{u}_m$ = 10 m s^{-1} (D, E, and F) on the β-plane. The black dots indicate the positions at 12-hour intervals.

In the above example, the vortex tracks converged when $\partial\bar{\zeta}_a/\partial y$ decreased towards the north, and diverged when $\partial\bar{\zeta}_a/\partial y$ increased towards the north. Thus, the convergence or divergence of the vortex tracks is determined by the sign of $\partial^2\bar{\zeta}_a/\partial y^2$. When $\bar{\zeta}_a$ is also a function of x, the convergence or divergence of the vortex tracks should depend on the sign of $\nabla^2\bar{\zeta}_a$ where ∇^2 is the horizontal Laplacian operator (the tracks will diverge for $\nabla^2\bar{\zeta}_a > 0$ and converge for $\nabla^2\bar{\zeta}_a < 0$). This can be understood physically by considering that the drift of the vortex is proportional to $\nabla\bar{\zeta}_a$. When the vector field $\nabla\bar{\zeta}_a$ is divergent ($\nabla^2\bar{\zeta}_a > 0$), the vortex tracks starting at different initial positions diverge, while the opposite is true when $\nabla\bar{\zeta}_a$ is convergent ($\nabla^2\bar{\zeta}_a < 0$).

The above result has implications for tropical cyclone track forecasting. For example, suppose a tropical cyclone moves into a region where $\nabla^2\bar{\zeta}_a > 0$. The subsequent track of the storm should then be fairly sensitive to the position at which the storm entered the region. Conversely, if a storm entered a region where $\nabla^2\bar{\zeta}_a < 0$, the subsequent track would not be so sensitive to the position where the storm entered the region. From the point of view of dynamic prediction, in regions where $\nabla^2\bar{\zeta}_a > 0$ it might be expected that the storm track would be sensitive to initial position errors, and also to errors in the analysis of the large-scale flow which might result in an error in the initial direction of storm motion.

Similarly, when $\nabla^2\bar{\zeta}_a < 0$, it might be expected that the storm track would not be as sensitive to these factors. Thus, $\nabla^2\bar{\zeta}_a$ might be used to give some qualitative information about the expected magnitude of the position error from a dynamical model forecast.

The zonal wind profiles shown in Fig. 5 were chosen so that the relative vorticity gradients would be fairly large and the divergence and convergence of the storm tracks could be easily seen in Fig. 6. In fact, the relative vorticity gradients are large enough that the absolute vorticity gradient is zero at y = 1150 km and y = 1900 km for $\bar{u}_m$ = 10.0 m s^{-1} and at y = 2100 km and y = 2850 km for $\bar{u}_m$ = −10.0 m s^{-1}, so that a necessary condition for barotropic instability is satisfied (Kuo, 1951). Since the onset of barotropic instability would act to reduce the magnitude of the absolute vorticity gradient, the observed absolute vorticity gradients in the regions of tropical cyclones might not be as large as the gradients shown in Fig. 5.

To get some idea of the observed magnitude, $\nabla^2\bar{\zeta}_a$ was computed from the operational data used to initialize the SANBAR model at 0000 GMT 2 September 1979, obtained from S. Goldenberg (personal communication, 1983). At this time, the model was used to predict the tracks of hurricanes David and Frederic which were centered at 21°N, 75°W and 14°N, 54°W, respectively. As described by Sanders *et al.* (1980), the current operational version of the SANBAR model uses deep layer-mean horizontal winds between 123.5 and 36.5°W longitude, 0°N and 55°N latitude as input for a barotropic vorticity equation. These wind data were objectively analyzed to an equally spaced mercator grid with an actual average grid spacing of about 140 km. The analyzed horizontal wind components were then used to calculate $\nabla\bar{\zeta}_a$ and $\nabla^2\bar{\zeta}_a$, where centered differences were used for all derivatives, except at the boundaries of the domain where one-sided differences were used.

In the model simulations, it is straightforward to calculate $\nabla^2\bar{\zeta}_a$ since the zonal flow is specified separately from the vortex. For the observational data, however, the distinction between the vorticity of the two tropical cyclones and the steering current is less well defined. In order to isolate the large-scale steering current, a nine point spacial smoother was applied to the objectively analyzed horizontal wind components. The spacial smoother was applied 20 times, which reduces the amplitude of 1000, 2000 and 4000 km waves by factors of about 0.02, 0.40 and 0.80, respectively. Assuming the length scales of the tropical cyclone vorticity fields are less than about 1000 km, this filtering procedure should eliminate most of the vorticity associated with the storms.

Figure 7 shows the horizontal wind (upper panel) and normalized Laplacian of the absolute vorticity field (lower panel) for the filtered SANBAR data. The Laplacian of the absolute vorticity was normalized by multiplying $\nabla^2\bar{\zeta}_a$ by D/β where D is an arbitrary length scale set equal to 1000 km and β is the northward gradient of the Coriolis parameter evaluated at 20°N. The contour interval in the lower panel of Fig. 7 is 1.0 nondimensional units and the positions of David and Frederic are indicated by the synoptic symbol for a tropical cyclone. For comparison, at points E and B in Fig. 5, $D/\beta\nabla^2\bar{\zeta}_a$ has a magnitude of about 5.0.

The lower panel of Fig. 7 shows that both storms are in regions where $\nabla^2\bar{\zeta}_a < 0$. From the previous discussion, the subsequent model storm tracks would not be so sensitive to initial position errors. At the time shown in Fig. 7, David (the storm just north of Cuba) was moving towards the northwest at about 5 m s^{-1}, while Frederic was moving towards the west-northwest at about 8 m s^{-1}. From Fig. 7 it can be seen that David is moving towards a region where $\nabla^2\bar{\zeta}_a < 0$ while Frederic is moving towards a region where $\nabla^2\bar{\zeta}_a > 0$. It might then be expected that the longer range forecast errors (48–72 hours) would be larger for Frederic than for David.

Figure 7 also shows that the maximum magnitude of $\nabla^2\bar{\zeta}_a$ in the regions of the storms is about 1.0, which is about five times less than the value for the zonal wind profile in Fig. 5. It can also be seen that there is an area about 1000 km northeast of David where $\nabla^2\bar{\zeta}_a > 3.0$, and an area 1500 km north of Frederic where $\nabla^2\bar{\zeta}_a < -2.0$. Thus, there are regions in the domain where the magnitude of $\nabla^2\bar{\zeta}_a$ is comparable to that in the example shown in Figs. 5–6.

The above discussion of Fig. 7 is highly speculative, and is included only to demonstrate how the $\nabla^2\bar{\zeta}_a$ field might be used, and that the observed magnitude of $\nabla^2\bar{\zeta}_a$ is comparable to that for the idealized zonal wind shown in Fig. 5. A direct comparison of the $\nabla^2\bar{\zeta}_a$ field and track forecast errors in a number of cases is needed to see if a relationship actually exists. The results from a preliminary study are discussed in Section 6.

b. Effect of vortex structure

In the idealized examples presented in Section 3, the axisymmetric vortex defined by (3.1) was used in each simulation. Kasahara and Platzman (1963) and others have shown that the drift of the vortex relative to the steering current depends on the structure of the vortex as well as on the absolute vorticity gradient.

In order to illustrate the sensitivity of the vortex track to the structure of the tangential wind field, a perturbation tangential wind V' given by

$$V' = V'_m\left(\frac{r}{r'_m}\right)\exp\tfrac{1}{2}\left[1-(r/r'_m)^2\right] \qquad (4.2)$$

was added to the axisymmetric vortex given by (3.1). Figure 8 shows $V + V'$ for V'_m = 30.0 m s^{-1}, r'_m = 40 km (I), V'_m = 5.0 m s^{-1}, r'_m = 300 km (S) and

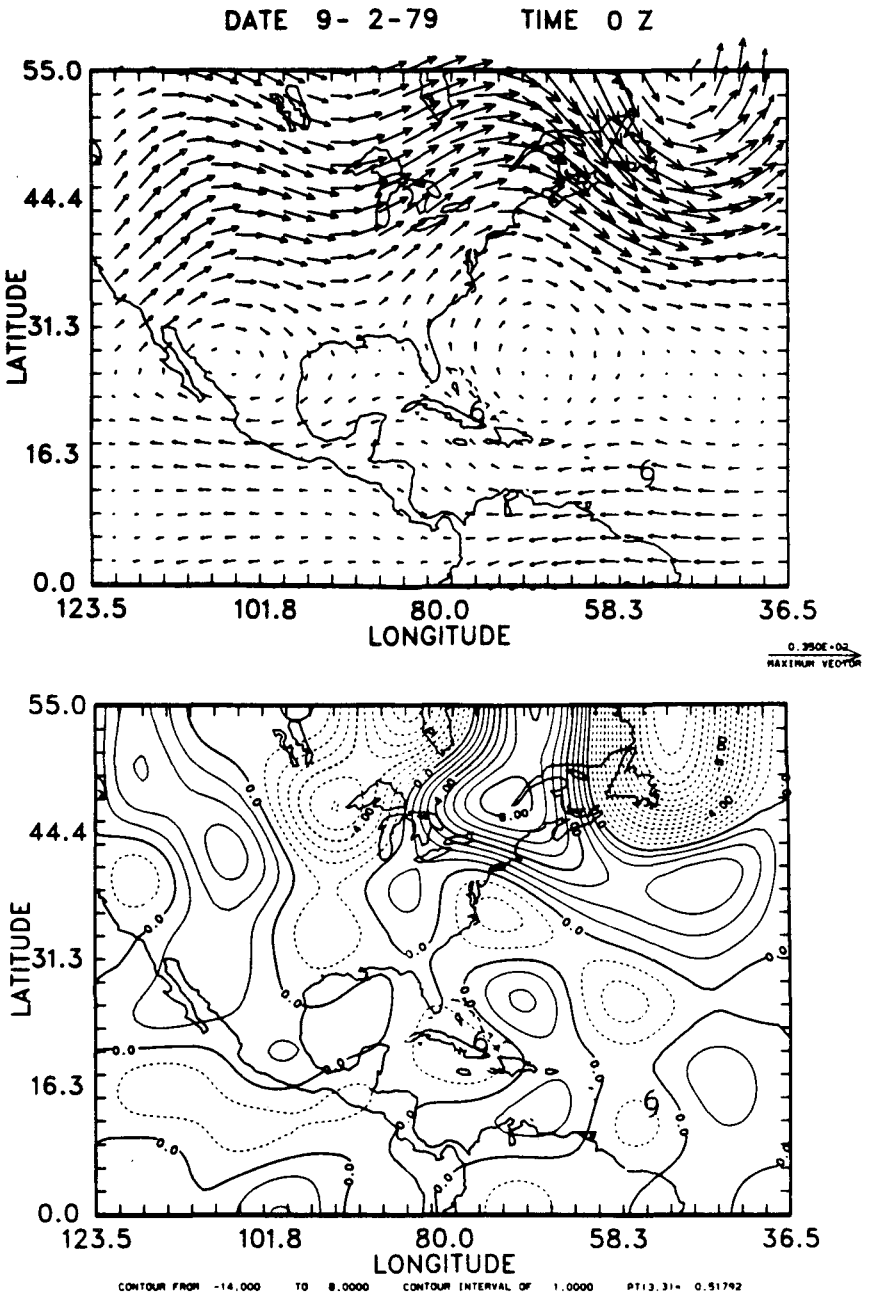

FIG. 7. The horizontal wind field (upper panel) and the normalized Laplacian of the absolute vorticity (lower panel) calculated from the filtered SANBAR data. The positions of hurricanes David and Frederic are indicated by the synoptic symbol for a tropical cyclone.

V'_m = 0.0 (C). These parameters were chosen so that profile (I) would represent an increase in the intensity of the control vortex (C), while profile (S) represents an increase in the size of the control vortex. Using the terminology of Holland (1984), an intensity change refers to a change in the maximum wind of a tropical cyclone without much change in the outer circulation, while a size change refers to a change in the outer circulation without much change in the maximum wind.

The three vortices shown in Fig. 8 were each centered at y_0 = 1500 km and y_0 = 500 km and the model was run with the sinusoidal zonal current shown in Fig. 3 and β evaluated at 20°N. Figure 9 shows the track of the vortex in each simulation, and the inset above each set of tracks shows the position

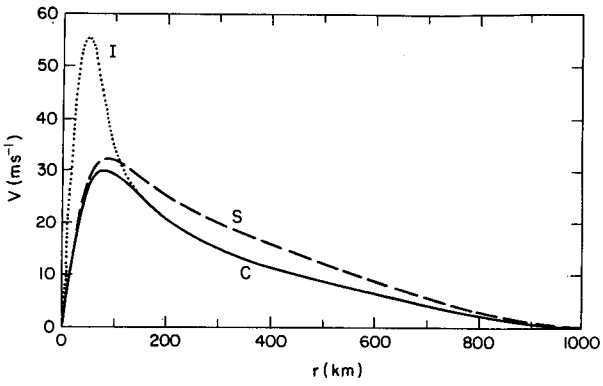

FIG. 8. The tangential wind V as a function of radius r for the vortex defined by (3.1) (C). Also shown are the sum of the vortex defined by (3.1) and the vortex defined by (4.2) with V'_m = 30 m s^{-1}, r_m = 40 km (I), or V'_m = 5.0, r'_m = 300 km (S).

difference between (I) and (C), and (S) and (C). This figure shows that track is much more sensitive to changes in the size of the vortex than to intensity changes. In fact, for y_0 = 500 km and y_0 = 1500 km, the position difference between vortices (I) and (C) remained less than 8 km during the 72-hour simulations. A result similar to this has been presented by Holland (1984), where the initial vorticity tendencies in a divergent barotropic model were considered.

Figure 9 also shows that for y_0 = 500 km, the position difference for |S − C| after 72 hours is about 90 km compared to about 140 km for y_0 = 1500 km. This indicates that the track of the vortex was more sensitive to size changes at y_0 = 1500 km than at y_0 = 500 km. This can be explained by considering the magnitude of $\nabla\bar{\zeta}_a$. As can be seen in Fig. 3, the gradient of the relative vorticity of the zonal current is the same at y_0 = 500 km and y_0 = 1500 km. As the vortex initially at y_0 = 1500 km moves northward, the relative vorticity gradient of the current at the vortex center decreases in magnitude, so that $\nabla\bar{\zeta}_a$ increases. As the vortex initially at y_0 = 500 km moves northward, however, the magnitude of $\nabla\bar{\zeta}_a$ decreases. Thus, the vortex initially at y_0 = 500 km moves through a region where the magnitude of $\nabla\bar{\zeta}_a$ is smaller than for the vortex initially at y_0 = 1500 km. Since the change of the vortex track due to the increase in the vortex size is related to $\nabla\bar{\zeta}_a$, the larger magnitude of $\nabla\bar{\zeta}_a$ for the y_0 = 1500 km vortex results in a greater sensitivity to size changes compared to the y_0 = 500 km vortex.

The sensitivity of the tropical cyclone track to the vortex size has been recognized in the development of operational models. In the moveable fine mesh (MFM) model used at NMC, a vortex is developed using a version of the model with no mean flow and then added to the three-dimensional large-scale analysis (Hovermale and Livezey, 1977). In an early version of the model, the vortex generated was unrealistically large which resulted in a poleward bias in the storm track. This was later corrected by adjusting the mixing coefficients so that a smaller initial vortex was produced. A result similar to this has been found in the Navy's nested tropical cyclone model (NTCM) where the inclusion of a larger initial vortex introduced a poleward bias in the storm track (Harrison and Fiorino, 1982).

Although adjustments have been made to make the initial vortex in operational models close to a climatological storm, the initial vortex is not dependent on the size of the observed storm (Elsberry, 1979). The above results suggest that the accuracy of a track forecast might be improved by making the initial vortex size a function of the observed storm size. The model results also indicate that it might not be as important to accurately specify the initial storm intensity.

The above results also indicate that the sensitivity of a tropical cyclone track to size changes depends on properties of the large-scale flow. For example, in regions where $|\nabla\bar{\zeta}_a|$ is large, it might be expected that the storm track would be sensitive to the vortex structure, while in regions of small $|\nabla\bar{\zeta}_a|$, the track would not be so sensitive to the vortex structure. Since the size of the vortex in operational models does not depend on the observed storm size, it might then be expected that the track forecast errors would be larger in regions where $|\nabla\bar{\zeta}_a|$ is larger. The preliminary results from a study which compares $|\nabla\bar{\zeta}_a|$ to forecast errors from an operational model are discussed in Section 6.

The above results also provide some justification for the use of the vortex shown in Fig. 1. This vortex was chosen so that the tangential wind at large radii

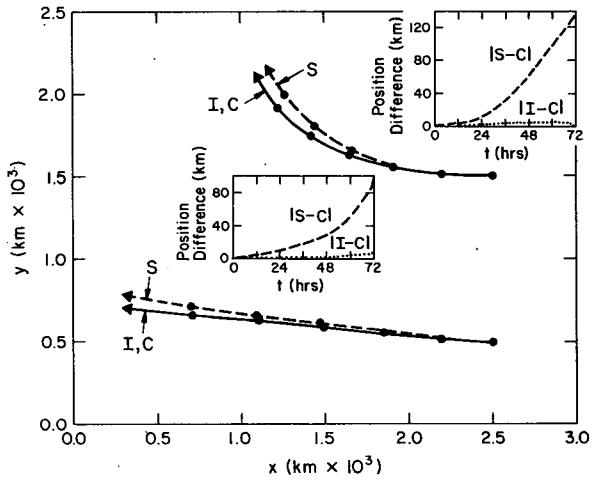

FIG. 9. The tracks of vortices C, I, and S when placed in the zonal current defined by (3.3) on the β-plane, where the black dots indicate the positions at 12-hour intervals. The insets above each set of tracks show the time evolution of the position difference between vortices (I) and (C), and vortices (S) and (C).

would be close to observed values. As seen in Fig. 1, however, the maximum tangential wind is only 30 m s^{-1} at a radius of 80 km. As shown by Shea and Gray (1973), the observed maximum tangential wind can be much larger than 30 m s^{-1} and the radius of maximum wind can be much less than 80 km. Since the track is not sensitive to changes in the inner regions, the model results using the vortex shown in Fig. 1 should be representative of much more intense storms.

5. Effect of numerical approximation

The accuracy of finite difference and spectral methods depends on the number of degrees of freedom. In operational models, the resolution used is determined by operational time constraints as well as by accuracy requirements. The grid spacing which is actually used ranges from about 140 km in the SANBAR model (Sanders *et al.*, 1980) to about 40 km in the NTCM (Harrison and Fiorino, 1982). Thus, some component of the track error in operational models is due to the numerical approximation of the solution. In this section, the second-order finite difference version of the barotropic model described in Section 2 is run with the resolution used in operational models and the results are compared with the results from the high resolution spectral model. In this way, the effect of numerical approximation on the vortex track can be estimated in a fairly simple context.

To determine the effect of resolution on the vortex track, the finite difference model was run with 67, 41, and 30 grid points in the x and y directions on a 4000 km square domain. The corresponding grid spacing in each of these simulations is 61 km, 100 km, and 138 km, respectively. For each of these simulations, the axisymmetric vortex defined by (3.1) was added to the sinusoidal zonal current given by (3.3) at $x_0 = 2500$ km, $y_0 = 1500$ km and the model was run for 72 hours with β evaluated at 20°N. This is the same initial condition used in the control simulation for the size and intensity change experiments. The track of the vortex in the spectral model for this initial condition is indicated by the solid line in the upper set of tracks in Fig. 9.

The spectral model was truncated at wavenumber 47 in all of the previous simulations. As will be seen later, when the wavenumber truncation is decreased to 33, the track of the control vortex changes very little. (The maximum position difference in the two simulations is less than 10 km.) This indicates that the wavenumber 47 solution is very close to the true solution. Thus, the errors in the finite difference model were assessed by comparing the results to the wavenumber 47 spectral solution.

Table 1 shows the position difference at 24, 48 and 72 hours between the vortex in the spectral model and the finite difference model with grid spacings of 61 km, 100 km and 138 km. This table shows that for $\Delta x = 61$ km, the position difference remains below about 110 km. The average position errors for operational forecasts in the Atlantic region are about 400 km and 600 km at 48 hours and 72 hours respectively (Neumann and Pelissier, 1981a). Since the operational errors are much larger than the errors introduced by the use of a second-order finite difference method, a grid spacing of about 60 km might be considered adequate.

When the grid spacing is increased to 100 km and 138 km, the position differences shown in Table 1 become very large. In fact, after 24 hours, it was no longer possible to locate a vorticity maximum associated with the vortex. Thus, for the size of the vortex used here, these grid spacings are inadequate. A possible solution to this problem would be to use a larger initial vortex so that it could be better resolved. As discussed previously, however, this would result in a poleward bias in the storm tracks.

For comparison, the resolution of the spectral model was also reduced and the errors in the track were assessed by comparing the results to the $N = 47$ simulation. For this purpose, the spectral model was truncated at $N = 33$, $N = 20$, and $N = 14$. For $L = 4000$ km the corresponding grid spacings of the shortest resolved waves ($2\Delta x$) are $\Delta x = 61$ km, 100 km and 143 km, respectively. Table 1 shows the position errors introduced by decreasing the resolution in the spectral model. As expected, the spectral model introduces much smaller errors in the vortex track compared to the finite difference model with corresponding resolution.

Orszag (1971) indicated that the principal source of inaccurate results in finite difference models for flows dominated by advection comes from phase errors (the short wavelength part of the solution is

TABLE 1. The position error in kilometers introduced using various spacial resolutions in the finite difference and spectral models.

Forecast (h)	Finite difference model			Spectral model		
	$\Delta x = 61$ km	$\Delta x = 100$ km	$\Delta x = 138$ km	$N = 33$	$N = 20$	N = 14
24	109	225	380	1	9	19
48	62	—	—	5	33	79
72	105	—	—	8	92	192

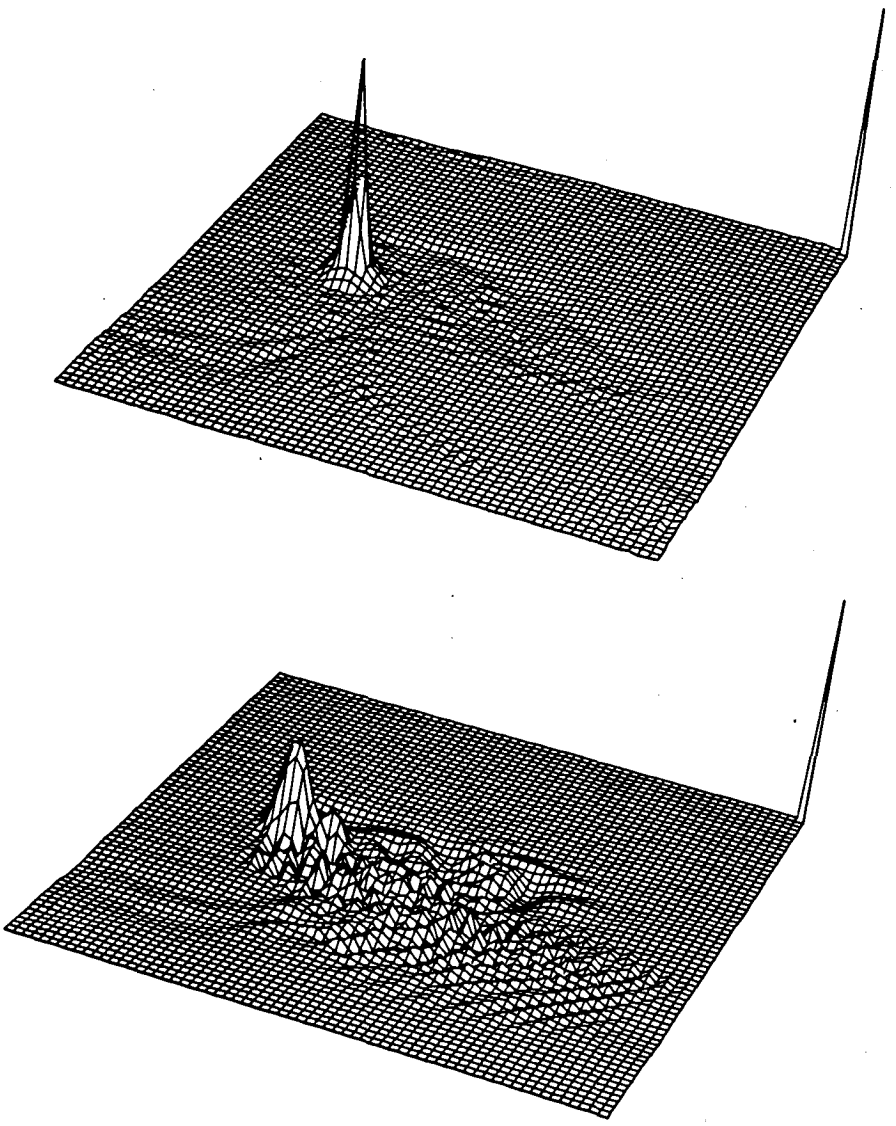

FIG. 10. The relative vorticity field normalized by the Coriolis parameter at 20°N at 72 hours for the $N = 33$ spectral model (upper), and $\Delta x = 61$ km finite difference model (lower). The model domain is viewed from the southeast and the point in the northeast corner was set to 30 nondimensional units.

advected too slowly). This results in computational dispersion which can distort the field which is being advected. To illustrate this effect, Fig. 10 shows the relative vorticity field at 72 hours displayed as a three-dimensional surface for the spectral model ($N = 33$) and the finite difference model ($\Delta x = 61$ km). This figure shows that the vorticity of the vortex has a fairly sharp peak compared to the vorticity in the rest of the domain. The $N = 33$ spectral solution conserves the vorticity peak fairly well. For the $\Delta x = 61$ km finite difference solution, however, the amplitude of the peak is reduced by 72 hours, and the effect of the computational dispersion can be seen. For $\Delta x = 100$ km and 138 km, the dispersion was so severe that the vorticity peak associated with the vortex could no longer be identified after 24 hours.

6. Concluding remarks

In this paper, the motion of tropical cyclones was investigated in the context of the nondivergent barotropic model. In Section 3, the results from the studies in the 1950s and 1960s were summarized and verified using idealized model simulations. It was shown that in the absence of steering current vorticity gradients, an axisymmetric vortex moves with steering

current velocity at the vortex center. It was also shown that the absolute vorticity gradient of the steering current ($\nabla\bar{\zeta}_a$) causes the vortex to drift relative to the current with a component in the direction of the gradient, and a component 90° to the left of the gradient.

In Section 4, the implications of the results of Section 3 for operational track prediction models were discussed. It was shown that the track of a vortex will be more sensitive to initial position errors in regions where $\nabla^2\bar{\zeta}_a > 0$. It was also shown that the track of a vortex is more sensitive to the vortex size than the vortex intensity, and that the track is more sensitive to the vortex size in regions where $|\nabla\bar{\zeta}_a|$ is large.

The above results suggest that it would be useful to include some information about the size of a tropical cyclone in the initial condition in operational models. Since the vortex structure is not a function of the storm size in current models, the above results also suggest that track forecast errors might be larger in regions where $|\nabla\bar{\zeta}_a|$ is large. Since there are errors in the initial position of a storm, the above results also suggest that the track errors might be larger in regions where $\nabla^2\bar{\zeta}_a > 0$.

In a preliminary study, the track errors from the MFM and the NTCM for 11 cases of Atlantic tropical cyclones were correlated with $|\nabla\bar{\zeta}_a|$ and $\nabla^2\bar{\zeta}_a$ in the regions surrounding the storms. These results show that a statistically significant relationship exists between $|\nabla\bar{\zeta}_a|$ and the track forecast errors from the MFM. Using standard linear regression techniques with $|\nabla\bar{\zeta}_a|$ as the independent variable, 45% and 18% of the variance of the position errors at 24 and 48 hours were accounted for. Using the t-statistic, the above results were significant at the 98% and 81% levels, respectively. The results for $\nabla^2\bar{\zeta}_a$, however, were somewhat inconclusive. The difficulty appears to be related to the method used to calculate $\nabla^2\bar{\zeta}_a$. The details of this study will be reported at a later time.

In Section 5, the effect of numerical approximation on the motion of a tropical cyclone was investigated. These results showed that the phase errors in the finite difference model resulted in fairly large errors in the prediction of the tropical cyclone track, particularly when the resolution was equal to that used in the SANBAR model ($\Delta x \approx 140$ km). In this case, the phase errors were so large that the vorticity peak associated with the tropical cyclone was rapidly reduced by computational dispersion, so that a consistent vorticity maximum could no longer be tracked after 24 hours. When the grid spacing was reduced to 60 km (the grid spacing used in the MFM model), the track errors remained less than about 110 km during a 72-hour integration. These results indicate that the grid spacing used in operational models might be inadequate in some cases.

In this study, the processes which affect the motion of an axisymmetric vortex were illustrated by specific examples. Many of the results presented here are in qualitative agreement with the results presented by Kasahara and Platzman (1963). In their study, more quantitative results were obtained using properties of a barotropic vorticity equation and the assumption that an axisymmetric vortex moves in such a way that the distortion of the steering current is minimized. If the assumptions made by Kasahara and Platzman could be verified using numerical simulations, their theory could be used to give more quantitative information about the processes which affect the motion of an axisymmetric vortex.

Acknowledgments. The author would like to thank Stan Goldenberg for providing the SANBAR data. Valuable comments were also received from Jim Hack, Greg Holland, Akira Kasahara, Jim McWilliams, and Wayne Schubert. The manuscript was typed by Ursula Rosner.

REFERENCES

Adem, J., 1956: A series solution for the barotropic vorticity equation and its application in the study of atmospheric vorticities. *Tellus,* **8,** 364–372.

——, and P. Lezama, 1960: On the motion of a cyclone embedded in a uniform flow. *Tellus,* **12,** 255–258.

Anthes, R. A., 1982: *Tropical Cyclones: Their Evolution, Structure and Effects. Meteor. Monogr.,* No. 41, Amer. Meteor. Soc., 208 pp.

——, and J. E. Hoke, 1975: The effect of horizontal divergence and latitudinal variation of the Coriolis parameter on the drift of a model hurricane. *Mon. Wea. Rev.,* **103,** 757–763.

Arakawa, A., 1966: Computational design for long-term numerical integrations of the equations of atmospheric motion. *J. Comput. Phys.,* **1,** 119–143.

Chan, J. C. L., 1984: An observational study of the physical processes responsible for tropical cyclone motion. *J. Atmos. Sci.,* **41,** 1036–1048.

Birchfield, G. E., 1960: Numerical prediction of hurricane movement with the use of a fine grid. *J. Meteor.,* **17,** 406–414.

DeMaria, M., and W. H. Schubert, 1984: Experiments with a spectral tropical cyclone model. *J. Atmos. Sci.,* **41,** 901–924.

Elsberry, R. L., 1979: Applications of tropical cyclone models. *Bull. Amer. Meteor. Soc.,* **60,** 750–762.

Harrison, E. J., 1981: Initial results from the Navy two-way interactive nested tropical cyclone model. *Mon. Wea. Rev.,* **109,** 173–177.

——, and M. Fiorino, 1982: A comprehensive test of the Navy nested tropical cyclone model. *Mon. Wea. Rev.,* **110,** 645–650.

Holland, G. J., 1983: Tropical cyclone motion: Environmental interaction plus a beta effect. *J. Atmos. Sci.,* **40,** 328–342.

——, 1984: Tropical cyclone motion: A comparison of theory and observation. *J. Atmos. Sci.,* **41,** 68–75.

Hovermale, J., and R. E. Livezey, 1977: Three-year performance characteristics of the NMC hurricane model. *Preprints 11th Tech. Conf. on Hurricanes and Tropical Meteorology,* Miami Beach, Amer. Meteor. Soc., 122–125.

Jones, R. W., 1977: Vortex motion in a tropical cyclone model. *J. Atmos. Sci.,* **34,** 1518–1527.

Kasahara, A., 1957: The numerical prediction of hurricane movement with the barotropic model. *J. Meteor.,* **14,** 386–402.

——, and G. W. Platzman, 1963: Interaction of a hurricane with the steering flow and its effect upon the hurricane trajectory. *Tellus,* **15,** 321–335.

Kitade, T., 1980: Numerical experiments of tropical cyclones on a plane with variable Coriolis parameter. *J. Meteor. Soc. Japan,* **58,** 471–488.

——, 1981: A numerical study of the vortex motion with barotropic models. *J. Meteor. Soc. Japan,* **59,** 801–807.

Kuo, H. L., 1950: The motion of atmospheric vortices and the general circulation. *J. Meteor.,* **7,** 247–258.

——, 1951: Dynamical aspects of the general circulation and the stability of zonal flow. *Tellus,* **3,** 268–284.

——, 1969: Motion of vortices and circulating cylinder in shear flow with friction. *J. Atmos. Sci.,* **26,** 390–398.

Madala, R. V., and S. A. Piacsek, 1975: Numerical simulation of asymmetric hurricanes on a β-plane with vertical shear. *Tellus,* **27,** 453–468.

Merrill, R. T., 1984: A comparison of large and small tropical cyclones. *Mon. Wea. Rev.,* **112,** 1408–1418.

Neumann, C., and J. Pelissier, 1981a: An analysis of Atlantic tropical cyclone forecast errors, 1970–79. *Mon. Wea. Rev.,* **109,** 1248–1266.

——, and ——, 1981b: Models for the prediction of tropical cyclone motion over the North Atlantic: An operational evaluation. *Mon. Wea. Rev.,* **109,** 522–538.

Orszag, S. A., 1971: Numerical simulation of incompressible flows within simple boundaries: Accuracy. *J. Fluid Mech.,* **49,** 75–112.

Riehl, H., and N. M. Burgner, 1950: Further studies on the movement and formation of hurricanes and their forecasting. *Bull. Amer. Meteor. Soc.,* **31,** 244–253.

Rossby, C. G., 1948: On displacement and intensity changes of atmospheric vortices. *J. Mar. Res.,* **7,** 175–187.

Sanders, F., and R. W. Burpee, 1968: Experiments in barotropic hurricane track forecasting. *J. Appl. Meteor.,* **7,** 313–323.

——, A. L. Adams, N. J. B. Gordon and W. D. Jensen, 1980: Further development of a barotropic operational model for predicting paths of tropical storms. *Mon. Wea. Rev.,* **108,** 642–654.

Sasaki, Y., 1955: Barotropic forecasting for the displacement of typhoon. *J. Meteor. Soc. Japan,* **33,** 1–8.

Shea, D. J., and W. M. Gray, 1973: The hurricane's inner core region. I. Symmetric and asymmetric structure. *J. Atmos. Sci.,* **30,** 1544–1564.